JOURNAL OF GEOPHYSICAL RESEARCH, VOL. ???, XXXX, DOI:10.1002/,

The interaction between gravity waves and solar tides in a linear tidal model with a 4D ray-tracing gravity-wave parameterization

B. Ribstein[1] and U. Achatz[1]

Corresponding author: B. Ribstein, Institut für Atmosphäre und Umwelt, Johann Wolfgang Goethe Universität Frankfurt, Altenhöferallee 1, Germany. ribstein@iau.uni-frankfurt.de

[1]Institut für Atmosphäre und Umwelt,

Johann Wolfgang Goethe Universität

Frankfurt, Frankfurt-am-Main, Germany.

Abstract. Gravity waves (GWs) play an important role in atmospheric dynamics. Due to their short wavelengths they must be parameterized in current weather and forecast models, that cannot resolve them explicitly. We are here the first to report the possibility and the implication of having an on-line GW parameterization in a linear but global model that incorporates their horizontal propagation, the effects of transients and of horizontal background gradients on GW dynamics. The GW parameterization is based on a ray-tracer model with a spectral formulation that is safe against numerical instabilities due to caustics. The global model integrates the linearized primitive equations to obtain solar tides (STs), with a seasonally dependent reference climatology, forced by a climatological daily cycle of the tropospheric and stratospheric heating, and the (instantaneous) GW momentum and buoyancy flux convergences resulting from the ray-tracer. Under a more conventional *"single-column"* approximation, where GWs only propagate vertically and do not respond to horizontal gradients of the resolved flow, GW impacts are shown to be significantly changed in comparison with "full" experiments, leading to significant differences in ST amplitudes and phases, pointing at a sensitive issue of GW parameterizations in general. In the "full" experiment, significant semi-diurnal STs arise even if the tidal model is only forced by diurnal heating rates. This indicates that an important part of the tidal signal is forced directly by GWs via their momentum and buoyancy deposition. In general the effect of horizontal GW propagation and the GW re-

sponse to horizontal large-scale-flow gradients is rather observed in non-migrating than in migrating tidal components.

1. Introduction

Internal gravity waves (GWs) are of great importance for atmospheric and oceanic dynamics, as testified by the recent number of review papers [e.g. *Plougonven and Zhang*, 2014; *Vanneste*, 2013; *Ivey et al.*, 2008; *Fritts and Alexander*, 2003; *Kim et al.*, 2003]. GW dynamics still needs to be parameterized in general circulation models, including climate models, because explicitly resolving the whole GW spectrum is beyond our present-day computational capabilities (as recently shown for the atmosphere by *Liu et al.* [2014]).

In both the atmosphere and the oceans, the large-scale impact of GWs arises from wave-mean flow interaction and/or mixing. Turbulent mixing due to GW instabilities significantly contributes to the closure of the thermohaline circulation [see e.g. the review *Ivey et al.*, 2008]. GW-momentum deposition explains the meridional mesopheric circulation, and the associated increase of temperature from summer to winter hemisphere [*Holton*, 1982], and contributes essentially to the quasi-biennial oscillation (QBO) in the stratosphere. GWs also provide an important dynamic link between their source levels, primarily the troposphere and lower stratosphere, and their breaking altitudes, primarily in the upper stratosphere and in the mesosphere.

Current GW parameterizations give reasonable results in the troposphere and lower stratosphere, in climate and weather forecast models in comparison with observation, showing e.g. similar statistics and distribution [*de la Camara et al.*, 2014]. GW amplitudes are nevertheless still tuned in those models to reproduce the appropriate large-scale circulation of the atmosphere. Optimal values turn out to be approximately 5 times weaker than those from in-situ measurement [*Jewtoukoff et al.*, 2015]. In addition, as climate and weather forecast models increasingly encompass the whole middle atmosphere (e.g. *Schmidt et al.* [2006], *Marsh et al.* [2013]) nowadays GW parameterizations may describe GW dynamics with insufficient accuracy. Current GW parameterizations do not resolve their vertical propagation, but use an "instantaneous" vertical equilibrium profile of GW amplitudes from the source level to the model top, as detailed for example by *Lott and Guez* [2013] in the description of their parameterization. Amplitudes beyond some instability threshold, e.g. for static instability, trigger a wave-breaking parameterization that reduces the wave amplitude to or below the instability threshold. This then enables momentum deposition. Such an approach neglects the effect of the time dependence of the large-scale flow on the GWs, and of GW transience on the large-scale flow. The same holds for the effect of horizontal GW propagation. These two points have been shown to potentially play an important role, for example in the interaction between atmospheric solar tides (STs) and GWs [*Senf and Achatz*, 2011; *Ribstein et al.*, 2015]. In addition, the transient GW forcing of the mean-flow necessarily implies a time-dependent wave-induced large-scale flow. In idealized studies *Fritts and Dunkerton* [1984] and *Sutherland* [2001], e.g., have shown that the interaction between a GW and the wave-induced mean-flow can strongly modify wave propagation, through a phenomenon known as self-acceleration.

In a step away from idealized settings towards the application of a generalized GW model in a more realistic framework, the present work studies the dynamics of GWs in the middle atmosphere in a global tidal model. STs are global waves driven by the daily cycle of direct solar heating [*Lindzen and Chapman*, 1969] and various other heat tropospheric and stratospheric heat sources [e.g. *Hagan and Forbes*, 2002]. None of these are purely sinusoidal at 24h period, so that STs present diurnal and sub-diurnal periodicity [studied e.g. by *Forbes and Wu*, 2006; *Zhang et al.*, 2006]. Just like GWs, STs contribute significantly both to the dynamics of the mesosphere and lower-thermosphere (MLT) and to the coupling between the troposphere and higher atmospheric layers.

In an attempt to incorporate the effects of GW vertical and horizontal propagation into our GW parameterization, GW dynamics is described using a ray-tracer model for the three-dimensional propagation on a global-scale flow based on *Ribstein et al.* [2015]. The eikonal equation used there naturally emerge from the analytical study of the interaction with a large-scale balanced time-evolving flow [*Bretherton*, 1966; *Andrews and McIntyre*, 1978a, b; *Buhler*, 2009; *Achatz et al.*, 2010]. Moreover, following the findings of *Muraschko et al.* [2015], a special description of GW amplitudes has been implemented [*Buhler and McIntyre*, 1999; *Hertzog et al.*, 2002] that helps avoiding numerical instabilities due to *caustics*, otherwise classical limitation of the *Wentzel-Kramers-Brillouin* (WKB) theory, see e.g. the review from *Broutman et al.* [2004] on ray-tracer models for internal waves in the atmosphere and oceans. Without this special description of GW amplitudes, even an initially locally monochromatic GW field quickly develops numerical instabilities.

The global tidal model is based on *Grieger et al.* [2004]; *Achatz et al.* [2008], and has also been used in *Ribstein et al.* [2015]. Linear models have the advantage of allowing a clearer cause-effect relationship, as will be of use below in the identification of the role of GWs in forcing the semidiurnal ST. The first very important difference to *Ribstein et al.* [2015] consists in how GW effects are accounted for in the linear tidal model. In that study effective Rayleigh-friction and Newtonian-relaxation coefficients had been determined, via linear regression, from ray-tracer data, and these have then been used to represent the GW effect in the linear diurnal model. Here, however, the GW drags are used directly as a forcing of diurnal and sub-diurnal STs. The second major difference to *Ribstein et al.* [2015] consists in how GWs and STs are coupled. In the present study we do not follow the procedure and methodology of *Meyer* [1999], where the GWs-STs interaction was taken into account by iteratively running the two models. Thus, in *Ribstein et al.* [2015], the tidal model sees as GW impact the aforementioned Rayleigh-friction and Newtonian-relaxation coefficients, and yields a solution for the STs that is then used in the ray-tracer as time dependent three dimensional background. From the hence resulting ray-tracer data new Rayleigh-friction and Newtonian-relaxation coefficients are determined that are to be used in a next iteration of the tidal model, and so forth. In the present study, however, the ray-tracer model and the linear tidal model interact at each time step, allowing so GWs to interact with the wave-induced large-scale flow. In essence, the present study therefore represents the first implementation of the methodology of *Muraschko et al.* [2015] in a global atmosphere model, with an additional incorporation of the effects of GW horizontal propagation. The ray tracer is used directly as a GW parameterization for the linear global tidal model.

For the presentation of our investigations with this kind of coupled model, section 2 gives a description of both the global linear model and the ray-tracer model. Section 3 then presents results from both the global model and our GW parameterization, shown together with those using a more conventional parameterization of GWs. A summary is finally given in section 4.

2. Model Description

The ray-tracer model assumes a slowly varying background flow on which the GWs propagate, consistently with the WKB ansatz. That background flow consists of a monthly-mean climatology and STs propagating on the latter, simulated by the linear tidal model and forced by climatological radiative fluxes as by the GW forcing due to the convergences of GW momentum and buoyancy fluxes. The monthly-mean climatological fields had been obtained from data from a 20-year run of the global circulation model HAMMONIA [see e.g. *Schmidt et al.*, 2006]. The corresponding zonal wind U_{BG} and temperature T_{BG} fields are plotted in Fig. 1, showing their annual-cycles and zonally-averaged December-profiles. Because the zonally-averaged climatological fields are close to balanced, the increase of temperature from winter to summer hemisphere in the mesosphere should there be linked to the closure of the mesospheric jets, both visible in Fig. 1.

The linear global tidal model, as the ray-tracer model used in the present study are in many regards similar to those used in *Ribstein et al.* [2015], described there in detail. In sections 2.1 and 2.2, we therefore focus more on respective changes due to the modified coupling.

2.1. Tidal model

The linear tidal model is the linearization of a primitive equation global model (details of the original model in *Becker and Schmitz* [2003]) about some arbitrary reference state, here the monthly-mean climatology.

The discretized atmosphere is decomposed into a reference-state part Y_0, all tidal components Y_{ST} and the remaining transients. At any combination of latitude and altitude, the spatio-temporal distribution corresponding to Y_{ST} can be decomposed using a time t and longitude λ Fourier transform,

$$\sum_{n=1}^{\infty}\sum_{s\in\mathbb{Z}}\left(\hat{Y}_{ST}(n,s)e^{i(n\Omega_T t+s\lambda)}+\hat{Y}_{ST}(n,s)^{*}e^{-i(n\Omega_T t+s\lambda)}\right) \tag{1}$$

where Ω_T is the Earth's rotation rate. Diurnal, semi-diurnal and ter-diurnal STs, respectively, correspond to oscillations with $(24h, 12h, 8h)$ period, are denoted by $n = (1, 2, 3)$. Eastward propagation correspond to a negative zonal wavenumber s, respectively westward propagation for $(s > 0)$. Tides following the apparent westward solar motion $(s = n)$ are named migrating STs, and all the others constitute the non-migrating STs. The complex tidal amplitude $\hat{Y}_{ST}(n, s)$ and its complex conjugate $\hat{Y}_{ST}(n, s)^{*}$ are both latitude-altitude and seasonally dependent.

The linearization of the primitive-equation tendencies about some reference state Y_0 yields the linear operator $\mathcal{L}_0 Y_{ST}$, for any input Y_{ST}. The reference state is given by the aforementioned monthly-mean climatological fields obtained from the HAMMONIA data. $\mathcal{L}_0 Y_{ST}$ includes the directly linear dynamical terms in the primitive-equation tendencies but also the result of the linearization of the nonlinear contributions about Y_0. Stationary planetary waves, included in the monthly-mean climatology state vector Y_0, therefore interact with STs. As in *Ribstein et al.* [2015], the only dissipative process added is a molecular thermal conductivity.

The model is forced by the monthly-mean daily cycle of the heating rates $\mathcal{Q}$, again obtained from the HAMMONIA data. In contrast to *Ribstein et al.* [2015], both the diurnal $\mathcal{Q}(n = 1)$ and semi-diurnal $\mathcal{Q}(n = 2)$ components will be used here. In *Ribstein et al.* [2015], the GW impact has only been accounted for through (latitude-altitude and seasonally dependent) Rayleigh-friction and Newtonian-relaxation coefficients $(\gamma^{\mathcal{R}}, \gamma^{\mathcal{I}})$, obtained by regression of the GW momentum-flux and buoyancy-flux convergences in ray-tracer data onto diurnal STs and their tendencies. The resulting prognostic equations of the tidal model have been

$$\left(1 + \frac{\gamma^{\mathcal{I}}}{\Omega_T}\right)\partial_t Y_{ST} = \left(\mathcal{L}_0 - \gamma^{\mathcal{R}}\right) Y_{ST} + \mathcal{Q} \tag{2}$$

In the present study, the GW momentum-flux and buoyancy-flux convergences, together representing a GW forcing $\mathcal{F}_{GW}$, are used directly to force the tidal model, so that its prognostic equations are

$$\partial_t Y_{ST} = \mathcal{L}_0 Y_{ST} + \mathcal{F}_{GW} + \mathcal{Q} \tag{3}$$

As *Ribstein et al.* [2015] only used diurnal heating rates $\mathcal{Q}(n = 1)$, their linear model only resulted in diurnal STs as well, as seen from Eq. (2). In the present study, because $\mathcal{F}_{GW}$ is not constrained to be purely diurnal and regardless the climatological forcing used, solving Eq. (3) results in diurnal and non-diurnal STs. When only diurnal heating rates $\mathcal{Q}(n = 1)$ is used, the later therefore gives a measure of the GW influence on STs.

Our linear tidal model has a spectral truncation at $T14$ and uses 67 vertical levels. Eq. (3) is integrated by use of a fourth order scheme with a fixed time step of $\Delta t = 120s$. Together with the ray tracer, the model is integrated in total over 25 days, with heating $\mathcal{Q}$ increasing gradually during the first day. The last 5 days are used for a determination of the semidiurnal and diurnal STs by Fourier analysis.

2.2. GW model

The WKB ansatz underlying the ray-tracer model consists in describing a GW by a slowly varying amplitude, absolute frequency ω, and wavenumber vector $\mathbf{k} = k\mathbf{e}_\lambda + l\mathbf{e}_\theta + m\mathbf{e}_\mathbf{r}$, where $\mathbf{e}_\lambda$, $\mathbf{e}_\theta$ and $\mathbf{e}_\mathbf{r}$ denote the usual longitudinal, meridional and vertical unit vectors.

The GW ray-tracer model uses the local dispersion relation

$$\Omega(\mathbf{x},\mathbf{k},t) = \omega = \mathbf{k} \cdot \mathbf{U} \pm \sqrt{\frac{N^2(k^2+l^2)+f^2m^2}{k^2+l^2+m^2}} \tag{4}$$

and the corresponding Boussinesq polarization relations between the GW amplitudes in the various dynamical fields. The local latitude-dependent Coriolis parameter is denoted $f(\theta)$. Due to STs, the Brunt-Vaisala frequency $N(\mathbf{x},t)$ evolves in time and space, as are also the horizontal background wind components $\mathbf{U}(\mathbf{x},t) = U\mathbf{e}_\lambda + V\mathbf{e}_\theta$. The spatio-spectral time development of the GW field is obtained by following it along characteristics, so-called rays, given by

$$d_t\mathbf{x} = \mathbf{c_g} \tag{5}$$
$$d_t\mathbf{k} = -\nabla_\mathbf{x}\Omega \tag{6}$$

where $d_t = \partial_t + \mathbf{c_g} \cdot \nabla_\mathbf{x}$ is the time derivative along a ray, and $\mathbf{c_g} = \nabla_\mathbf{k}\Omega = c_{g\lambda}\mathbf{e}_\lambda + c_{g\theta}\mathbf{e}_\theta + c_{gz}\mathbf{e_r}$ denotes the absolute group velocity. Here $\nabla_\mathbf{x}$ ($\nabla_\mathbf{k}$) denotes the spatial (wavenumber) gradient.

The geometric position $\mathbf{x}$ and the wavenumber vector $\mathbf{k}$ evolve during the propagation. Projecting Eqs. (5) and (6) on spherical coordinates leads to the governing equations of GW propagation (see equations in *Ribstein et al.* [2015]). The ray-tracer model integrates Eqs. (5) and (6) along each ray path, where each ray is integrated forward separately. During the propagation, we do not allow rays to cross the poles.

In standard GW parameterizations, the horizontal wavenumber evolution due to background-flow horizontal gradients is neglected, as is the horizontal ray propagation. Under an approximation closer to conventional GW parameterizations, labeled here "*single-column*", we impose

$$d_t\lambda = d_t\theta = d_t k = d_t l = 0 \tag{7}$$

The curvature terms due to the spherical geometry have also been ignored in such an approximation (see *Ribstein et al.* [2015] for more details). It should be stressed that transient effects are taken into account in the single-column approximation, which would not be the case in conventional GW parameterizations.

In the absence of forcing and dissipation, the amplitude of a locally monochromatic GW is controlled by the conservation relation

$$\partial_t A + \nabla_{\mathbf{x}} \cdot (A\mathbf{c_g}) = d_t A + A\nabla_{\mathbf{x}} \cdot \mathbf{c_g} = 0 \tag{8}$$

for the wave-action density $A(\mathbf{x}, t)$, defined as the ratio between the energy E per unit of volume and the intrinsic frequency $\hat{\omega} = \omega - \mathbf{k} \cdot \mathbf{U}$ [e.g. *Grimshaw*, 1975]. The divergence of the group velocity $\nabla_{\mathbf{x}} \cdot \mathbf{c_g}$ determines the evolution of $A(\mathbf{x}, t)$, but as demonstrated by *Muraschko et al.* [2015], even an initially locally monochromatic GW field is prone to quickly develop multi-valued wavenumbers along so-called caustics, leading to numerical instabilities in a model that attempts to enforce monochromaticity.

In order to avoid these numerical instabilities we follow the procedure suggested by *Muraschko et al.* [2015] and expand the wave-action density in wave-number space by

$$A(\mathbf{x}, t) = \int_{\mathbf{k}\in\mathbb{R}^3} \mathcal{N}(\mathbf{x}, \mathbf{k}, t)\mathrm{d}\mathbf{k} \tag{9}$$

using a so called phase-space wave-action density $\mathcal{N}(\mathbf{x}, \mathbf{k}, t)$ that is conserved along the rays, i.e. it satisfies

$$\partial_t \mathcal{N} + \mathbf{c_g} \,\mathbf{.}\, \nabla_\mathbf{x} \mathcal{N} + d_t \mathbf{k} \,\mathbf{.}\, \nabla_\mathbf{k} \mathcal{N} = 0 \tag{10}$$

The initial distribution, advected conservatively along the different rays, gives the distribution at any time $t > 0$. This procedure is discretized numerically by gathering rays in finite ray volumes $\mathrm{d}^3\mathbf{k}\mathrm{d}^3\mathbf{x}$ around a characteristic carrier ray, each with uniform phase-space wave-action density $\mathcal{N}(\mathbf{x}, \mathbf{k}, t)$. By Eq. (10) that uniformity is conserved. Because the position-wavenumber phase-space group velocity is divergence free, each ray volume moreover preserves its volume content in position-wavenumber phase-space, but arbitrary shape deformations are possible. In a second discretization step we here constrain each ray volume, however, to keep a rectangular shape, responding nonetheless, in a volume-preserving manner, to local stretching and squeezing. *Muraschko et al.* [2015], have tested this procedure successfully against large-eddy simulations, though in a simpler framework.

As in *Ribstein et al.* [2015], a fixed and horizontally homogeneous lower boundary condition for $\mathcal{N}$ is chosen at $25\,km$, where a small and highly idealized meso-scale GW spectral ensemble (see *Ribstein et al.* [2015] for details) is prescribed at the rate of one ray volume per grid-cell. Checks of the dependence of our results on the ray-volume content identified only qualitative changes.

Since the rays move freely in space, the background fields are interpolated to each ray location via a linear polygonal interpolation. In parallel to the time-integration of the tidal model, the time-integration of the ray Eqs. (5, 6, 10) uses a fourth order scheme with a fixed time step of $\Delta t = 120\,s$, supplemented by a procedure to minimize numerical errors and stabilize the scheme (details in *Senf and Achatz* [2011]). As in *Ribstein et al.* [2015]), a static-stability criterion on the phase-space wave-action density $\mathcal{N}$ is used to mimic nonlinear wave-breaking (no dissipation if $\mathcal{N} < \mathcal{N}_{Sat}$, otherwise $\mathcal{N}$ is reduced to $\mathcal{N}_{Sat}$). Comparisons with large-eddy simulations of breaking GWs, to be published elsewhere, show that this heuristic method is a useful approach for such purposes.

We follow the same method as in *Ribstein et al.* [2015] to obtain from the ray-tracer data the forcing of the large-scale flow represented by the tidal model. Integrating over the contribution of the different rays, and using the polarization relations, momentum and buoyancy fluxes are calculated. It should be stressed that due to rotation rays carry horizontal buoyancy fluxes ($\rho \mathbf{u}' b'$), while the vertical flux ($\rho w' b'$) still vanishes. After using a localized smoothing procedure, the convergence of those fluxes is calculated as

$$f_x \equiv -\frac{1}{\rho} \nabla_{\mathbf{x}} \cdot (\rho \mathbf{v}' u') \tag{11}$$

$$f_y \equiv -\frac{1}{\rho} \nabla_{\mathbf{x}} \cdot (\rho \mathbf{v}' v') \tag{12}$$

$$f_b \equiv -\frac{1}{\rho} \nabla_{\mathbf{x}} \cdot (\rho \mathbf{v}' b') \tag{13}$$

Positive values of $f_{x,y}$ (or f_b) are associated with a local acceleration (or heating) of the surrounding large-scale flow.

As the tidal model is formulated in a Eulerian perspective, we have chosen to directly use these forcings, as also derived by *Grimshaw* [1975]. In that paper it is shown that a change of perspective, from Eulerian mean to Lagrangian mean, entails replacement of the active fluxes by the Eliassen-Palm (pseudo-momentum) flux in the momentum equation. At least in the limit of small large-scale Rossby numbers the two approaches are equivalent [*Buhler*, 2009].

3. Model results

In the following we present some key results from the global linear tidal model with ray-tracer GW parameterization, as described in section 2. These are obtained from a few experiments with different set-ups.

The *"full"* experiments refer to coupled-model simulations with no additional assumptions. The contributions of GW horizontal propagation and of large-scale flow horizontal gradients are identified by comparisons with *"single-column"* experiments where GWs propagate only vertically and the horizontal wavenumber $\mathbf{k}_H$ does not evolve. The contribution of horizontal large-scale flow gradients on GW propagation is neglected there as well, as seen in Eq. (7). Single-column experiments use some simplifying assumptions common to conventional GW parameterizations. The vertical wavenumber m, however, is allowed to vary, in response to the generally time-dependent vertical gradients in the background flow.

We remark that conventional GW parameterizations go even beyond the single-column approximation. They use in addition a steady-state approximation where at each time step an instantaneous vertical equilibrium profile of the GW properties is determined, that would eventually result from a steady GW radiation from the source altitude, or rather lower boundary, into the atmosphere. The corresponding adjustment time scales with the ratio between the vertical extent of the model atmosphere and the dominant vertical group velocity. *Senf and Achatz* [2011] show that this approximation can additionally modify the model results significantly as well. Idealized investigations to be published elsewhere show that simulations of the vertical propagation of an initially monochromatic GW field by a ray-tracer compare favorably to corresponding wave-resolving large-eddy simulations, while a conventional GW parameterization cannot reproduce the observed wave-mean-flow interaction.

The different experiments also differ in the climatological radiative forcing used in the linear tidal model. In experiments with *diurnal* forcing, STs are climatologically forced by a purely diurnal forcing $\mathcal{Q}(n = 1)$. In contrast to this, in experiments with *semi-diurnal* and *diurnal* forcing, STs are climatologically forced by the sum of semi-diurnal and diurnal $\mathcal{Q}(n = 1) + \mathcal{Q}(n = 2)$ heating.

3.1. GW fluxes

We first present, in Fig. 2, the zonal momentum flux convergence f_x (Eq. 11) for different simulations with purely *diurnal* forcing, both for *"full"* experiments and under the *"single-column"* approximation.

The GW drag calculated by the ray-tracer model is used in the global model to force STs, as described by Eq. (3). The daily mean of this forcing does not affect the STs, as the model is linear. In a nonlinear model it would have an impact on the slowly developing background on which the STs propagate, hence allowing for an indirect effect on the latter. This effect is not accounted for in our coupled model. Nonetheless, it is of interest what influence the ray tracer would have. From the zonal-mean climatology shown in Fig. 1, the diurnal-mean of the GW zonal momentum flux f_x is expected to accelerate, respectively decelerate, the zonal-mean zonal wind in the mesosphere in the summer hemisphere, respectively winter hemisphere.

Fig. 2 shows the annual cycle of the zonal and daily mean f_x at $80km$ altitude, as well its December and May altitude-latitude profiles. Indeed, we obtain positive and negative values in the summer and winter mesosphere, respectively. Despite the many simplifications in our coupled model, such as the GW source or the linear nature of the ST model, we reproduce important aspects of the GW climatological impact. Fig. 2 also shows the zonal-mean diurnal amplitude of the GW zonal momentum-flux convergence $\|f_x\|_{day}$ from the two experiments. It is structurally similar to the daily mean obtain from the same experiments, showing similar amplitudes and altitude-latitude structures. GW momentum deposition seems to generally both impact the daily mean state and the STs.

Global GW data at MLT altitudes are presently not available to an extent allowing comparisons with our simulations, but interesting local measurement exist. [*Liu et al.*, 2013; *Riggin et al.*, 2016, e.g.] present a significant diurnal cycle for the GW zonal drag with amplitudes compatible to our results. Also in agreement with our results, they present a GW meridional drag stronger, but still comparable, to the zonal one.

Comparing the GW forcing from the *"full"* and *"single-column"* experiments, we find that both amplitudes and the overall altitude-latitude structures are very different. This is illustrated in Fig. 2 by the zonal mean of the daily mean f_x and of the diurnal amplitude of $\|f_x\|_{day}$. Only the seasonal cycle at $80km$ altitude (and below) shows some similarities between both experiments. This is partly consistent with preliminary results from *Senf and Achatz* [2011] and *Ribstein et al.* [2015]. In *Senf and Achatz* [2011], however, the ray-tracer was not coupled to a tidal model, but rather used the HAMMONIA tides as background, whereas *Ribstein et al.* [2015] did the coupling iteratively, via efficient Rayleigh friction and Newtonian relaxation, as explained previously. Both of these studies found the single-column approximation to have a significant effect. Somewhat in contrast to our results, however, it was found to generally enhance the GW momentum and buoyancy deposition. Our results here indicate that the GW driving of the diurnal

ST tends to be enhanced/reduced in the winter/summer mesosphere and thermosphere if the single-column approximation is dropped. Obviously the horizontal GW propagation and the GW response to horizontal gradients in the large-scale flow, admitted in our simulations, but not in the single-column approximation, leads to notable modifications.

In addition, Fig. 3 presents the zonal momentum-flux convergence f_x for the *"full"* experiments, either with purely diurnal $\mathcal{Q}(n=1)$ heating or with both diurnal and semi-diurnal $\mathcal{Q}(n=1)+\mathcal{Q}(n=2)$ heating in the tidal model. The zonal mean of both the daily mean and the diurnal amplitude $\|f_x\|_{day}$ are shown. The figure illustrates that the daily mean GW deposition of momentum and buoyancy is not affected much by the nature of the tidal heating. Notably, however, even in the purely diurnally forced experiment the amplitude $\|f_x\|_{1/2\ day}$ and the altitude-latitude structure of the semi-diurnal GW forcing is quite comparable with its diurnal counterpart. Therefore, even in the absence of semi-diurnal tidal heating, GW forcing induces some semi-diurnal and diurnal wave-induced large-scale flows of equal importance. This will be studied more in the next sub-section.

3.2. Solar tides

The STs obtained from the global tidal model are presented in Figs. 4 to 7, both for the *"full"* experiment and under the *"single-column"* approximation. Fig. 4 shows results from simulations with purely *diurnal* heating, whereas Figs. 5 to 7 show in addition results from each an experiment with both *semi-diurnal* and *diurnal* heating.

The diurnal STs have been decomposed, using Eq. (1), into their migrating and non-migrating part. The diurnal westward propagating ST denoted DW_1 constitutes the sun-synchronous diurnal migrating ST, the semi-diurnal westward propagating ST denoted

SW_2 constitutes the semi-diurnal migrating ST, and the respective rest forms the diurnal or semi-diurnal non-migrating STs.

The annual cycle of the DW_1 tidal amplitudes at $95km$ is shown in Fig. 4. The altitude is chosen in order to facilitate a comparison with satellites observation, e.g. Upper Atmosphere Research Satellite (UARS) wind observations [*Forbes et al.*, 2003; *Forbes and Wu*, 2006; *Zhang et al.*, 2006; *Forbes et al.*, 2007]. Given the linearity tidal model, and the over-simplified GW-source in the ray-tracer, no perfect agreement can be expected. Nonetheless, the *"full"* and *"single-column"* experiments still reveal an annual cycle of the diurnal migrating tide DW_1 that is similar to observations and the findings of *Ribstein et al.* [2015].

December and May altitude-latitude amplitude profiles for the meridional wind of the diurnal STs are presented in Fig. 4 as well. The overall structure of the profiles from the *"full"* and *"single-column"* experiments is quite similar. The amplitude of the non-migrating STs, however, differs considerably between the two experiments. The single-column approximation leads to a significant reduction of the amplitude of the non-migrating ST. As seen in Fig. 2 the corresponding zonal GW forcing is weaker as well, and it is rather limited to high latitudes. The same holds for the meridional GW forcing (not shown). Non-migrating STs have less forcing by solar heating than their migrating counterpart, GW forcing being therefore expected to cause a more visible contribution. The GW forcing in the *"single-column"* experiment is localized where non-migrating STs are weak. It appears that such a forcing is much less able to excite nonmigrating tides at significant amplitudes, as it projects much less on the tidal structures prescribed by the dynamics. This is not the case for the *"full"* experiment. It thus appears that the effect of the GWs enhancing the non-migrating ST in the *"full"* experiment rather cannot be captured by some efficient Rayleigh friction.

Figs. 5 and 6 show for December and May, respectively, the meridional wind of semi-diurnal STs. For SW_2, both the amplitude and the sine part (or imaginary part, see Eq. 1) are shown, and for the non-migrating component the zonal-mean amplitude. Results from simulations with purely *diurnal* heating in the linear tidal model are compared with those from a *"full"* experiment with both *semi-diurnal* and *diurnal* heating. Results for the corresponding *"single-column"* experiment are found to be quite similar (not shown) regarding the overall structure. As seen in Eq. 3, the linear tidal model with purely *diurnal* heating can yield non-diurnal STs only because of the GW impact, by their momentum and buoyancy deposition. Non-diurnal STs are in such simulations a clear measure of the GW influence on STs.

Interestingly in the *"full"* experiment, the overall altitude-latitude amplitude profiles of (the purely GW stimulated) SW_2 semi-diurnal ST shows some strong structural similarities with the one obtained by *semi-diurnal* and *diurnal* heating, although the strengths of the tidal amplitudes do differ. This is also the case, in December for example, for the zonal-mean profiles of the non-migrating ST. Notably, the non-migrating semi-diurnal ST due to the GW forcing seems to amount to about 50% of the total non-migrating ST, due to GW forcing and semi-diurnal heating in the tidal model. And the semi-diurnal component of the GW forcing tends to prefer certain non-migrating STs. Fig. 7 shows more details of the GW impact on STs, also in December. There, the non-migrating semi-diurnal STs are decomposed, using Eq. (1), into the standing semi-diurnal oscillation, denoted S_0, and the westward propagating STs denoted SW_1, respectively SW_3, with a zonal wavenumber $s = 1$, respectively $s = 3$. In particular, the figure shows that GW depositions contribute to more than 50% of the total S_0 tides, and to about 30% of the total SW_1 tidal component.

When the single-column approximation is applied, however, these structural similarities are lost. Moreover, it leads to a substantial reduction of the tidal amplitudes. The latter is even more pronounced than the corresponding effect on the non-migrating diurnal ST, as visible in Fig. 4. Therefore, contrary to *"single-column"* experiments, GWs in *"full"* simulations stimulate and significantly contribute to the non-migrating semi-diurnal STs.

4. Summary and Conclusions

GWs are of considerable dynamical importance for the atmosphere. This holds especially for the middle atmosphere where they drive the circulation to a significant part so that the mesospheric jets are closed, and that the coolest part of the atmosphere is above the summer pole. Similarly important is the role of GWs in the driving of the quasi-biennial oscillation in the stratosphere, and they have an all but negligible impact on STs. The latter is the focus of the present study. Many GWs being too small in scale to be resolvable by state-of-the-art climate models, and also global weather-forecast models, they present a parameterization problem that can partially be addressed using WKB theory, as done here. Beyond this, however, descriptions of GW dynamics focussing on its essential aspects, as provided by this theory, are and will remain valuable for the achievement of conceptual scientific understanding of atmospheric dynamics where GWs are involved.

We present here the first direct coupling between a WKB ray-tracer with a global-scale model, here for STs. Conventional GW parameterizations neglect the effects of transients and of horizontal background gradients on GW dynamics, as well as the ability of transient GWs to interact with the wave-induced large-scale flow. This is not the case in our three-dimensional ray-tracer model, used here to study the GW interaction with STs in a linear tidal model. We compare the results with those from a more traditionally used approximation in GW parameterization, named the *"single-column"* approximation, where GWs only propagate vertically, and where they do not respond to horizontal gradients of the resolved large-scale flow, to illustrate some limits of current GW parameterizations, but also to illustrate the dynamical importance of the interactions neglected there.

GW deposition of momentum and buoyancy is found to strongly differ, both in amplitude and overall structure, between runs under the single-column approximation, compared to those from the *"full"* experiment, where the wave-mean-flow interaction between scale-separated GWs and STs is treated without corresponding simplifications. Thus we find that admitting the effects of horizontal GW propagation and the GW response to horizontal gradients in the large-scale flow tends to enhance/reduce the GW driving of the diurnal ST in the winter/summer mesosphere and thermosphere. A central result also is the GW driving of the semi-diurnal ST that is identified even if the tidal model is only forced by diurnal heating. This effect virtually disappears in the single-column approximation.

The simulated STs exhibit corresponding features. The diurnal STs obtained from the coupled model, under diurnal heating, are found to differ considerably in amplitude between the two experiments. It should be highlighted that the single-column approximation leads to a significant reduction especially of the amplitude of the non-migrating STs. Moreover, under purely diurnal heating, and for the full experiment, the GWs alone stimulate semi-diurnal STs, showing, both for migrating and non-migrating STs, some strong structural similarities with the ones obtained under diurnal and semi-diurnal heating. Those similarities are not present under the single-column approximation, where the amplitudes of the semi-diurnal STs are negligibly small as a whole. In the full experiment, on the contrary, GW forcing contributes significantly to the semi-diurnal non-migrating STs. This effect is most prominent for the standing non-migrating component S_0.

In summary, we show that the effects of horizontal GW propagation and the GW response to horizontal gradients of the large-scale flow contribute significantly to the GW dynamics in the mesosphere. This is interesting both conceptually, e.g. with regard to the role of GW driving of non-migrating and semi-diurnal STs, and for GW parameterizations. Corresponding schemes relying on the single-column approach, although efficient, are in danger of yielding results of limited reliability. Explicit GW models might be a valuable alternative. The added numerical costs of such an approach are undoubtedly an issue that we have neglected so far on purpose. It seems appropriate to first investigate the impact of a generalized GW model on the results. Once demonstrated, one can turn towards efficiency issues. We hope that the time is approaching where the incentive to do so, using parallelism on high performance computers, gets strong enough. At least we hope that our results foster corresponding considerations and discussions.

Acknowledgments. The data for this paper are available upon request from the authors. B.R. and U.A. thank the German Federal Ministry of Education and Research (BMBF) for partial support through the program Role of the Middle Atmosphere in Climate (ROMIC) and through grant 01LG1220A. U.A. thanks the German Research

Foundation (DFG) for partial support through the research unit Multiscale Dynamics of Gravity Waves (MS-GWaves) and through grants AC 71/8-1, AC 71/9-1 and AC 71/10-1.

References

Achatz, U., N. Grieger, and H. Schmidt (2008), Mechanisms controlling the diurnal solar tide: Analysis using a gcm and a linear model, *J. Geophys. Res.*, *113*(A8), doi: 10.1029/2007JA012967.

Achatz, U., R. Klein, and F. Senf (2010), Gravity waves, scale asymptotics and the pseudo-incompressible equations, *J. Fluid Mech.*, *663*, 120–147.

Andrews, D. G., and M. E. McIntyre (1978a), An exact theory of the nonlinear waves on a lagrangian-mean flow, *J. Fluid Mech.*, *89*, 609–646.

Andrews, D. G., and M. E. McIntyre (1978b), On wave-action and its relatives, *J. Fluid Mech.*, *89*, 647664.

Becker, E., and G. Schmitz (2003), Climatological effects of orography and landsea heating contrasts on the gravity wavedriven circulation of the mesosphere, *J. Atmos. Sci.*, *60*, 103–118, doi:10.1175/1520-0469(2003)060¡0103:CEOOAL¿2.0.CO;2.

Bretherton, F. P. (1966), Propagation of groups of internal gravity waves in a shear flow, *QJRMS*, *92*(394), doi:10.1002/qj.49709239403.

Broutman, D., J. Rottman, and S. D. Eckermann (2004), Ray methods for internal waves in the atmosphere and ocean, *Annu. Rev. Fluid Mech.*, *36*, 233253, doi: 10.1146/annurev.fluid.36.050802.122022.

Buhler, O. (2009), *Waves and Mean Flows*, Cambridge Univ. Press.

Buhler, O., and M. E. McIntyre (1999), On shear-generated gravity waves that reach the mesosphere. part ii: Wave propagation, *J. Atmos. Sci.*, *56*, 3764–3773, doi: 10.1175/1520-0469(1999)056¡3764:OSGGWT¿2.0.CO;2.

de la Camara, A., F. Lott, and A. Hertzog (2014), Intermittency in a stochastic parameterization of nonorographic gravity waves, *J. Geophys. Res.: Atmospheres*, *119*, 11,905–11,919, doi:10.1002/2014JD022002.

Forbes, J., M. Hagan, and X. Zhang (2007), Seasonal cycle of nonmigrating diurnal tides in the MLT region due to tropospheric heating rates from the NCEP/NCAR reanalysis project, *Adv. Space Res.*, *39*(8), 1347–1350, doi:10.1016/j.asr.2003.09.076.

Forbes, J. M., and D. Wu (2006), Solar tides as revealed by measurements of mesosphere temperature by the MLS experiment on UARS, *J. Atmos. Sci.*, *63*, 1776–1797, doi: 10.1175/JAS3724.1.

Forbes, J. M., M. E. Hagan, S. Miyahara, Y. Miyoshi, and X. Zhang (2003), Diurnal nonmigrating tides in the tropical lower thermosphere, *Earth, Planets and Space*, *55*(7), 419–426.

Fritts, D. C., and M. J. Alexander (2003), Gravity wave dynamics and effects in the middle atmosphere, *Rev. Geophys.*, *41*(1), doi:10.1029/2001RG000106.

Fritts, D. C., and T. J. Dunkerton (1984), A quasi-linear study of gravity-wave saturation and self-acceleration, *J. Atmos. Sci.*, *41*, 3272–3289.

Grieger, N., G. Schmitz, and U. Achatz (2004), The dependence of the nonmigrating diurnal tide in the mesosphere and lower thermosphere on stationary planetary waves, *JASTP*, *66*(69), 733–754, doi:10.1016/j.jastp.2004.01.022.

Grimshaw, R. (1975), Nonlinear internal gravity-waves in a rotating fluid, *J. Fluid Mech.*, *71*, 497–512, doi:10.1017/S0022112075002704.

Hagan, M. E., and J. M. Forbes (2002), Migrating and nonmigrating diurnal tides in the middle and upper atmosphere excited by tropospheric latent heat release, *J. Geophys. Res.: Atmospheres*, *107*(D24), 1–15, doi:10.1029/2001JD001236.

Hertzog, A., C. Souprayen, and A. Hauchecorne (2002), Eikonal simulations for the formation and the maintenance of atmospheric gravity wave spectra, *J. Geophys. Res.: Atmospheres*, *107*(D12), 1–14, doi:10.1029/2001JC000815.

Holton, J. R. (1982), The role of gravity wave induced drag and diffusion in the momentum budget of the mesosphere, *J. Atmos. Sci.*, *39*, 791–799, doi:10.1175/1520-0469(1982)039¡0791:TROGWI¿2.0.CO;2.

Ivey, G. N., K. B. Winters, and J. R. Koseff (2008), Density stratification, turbulence, but how much mixing?, *Ann. Rev. Fluid Mech.*, *40*, 169–184, doi: 10.1146/annurev.fluid.39.050905.110314.

Jewtoukoff, V., A. Hertzog, R. Plougonven, A. de la Camara, and F. Lott (2015), Comparison of gravity waves in the southern hemisphere derived from balloon observations and the ecmwf analyses, *J. Atmos. Sci.*, *72*(9), 3449–3468, doi:10.1175/JAS-D-14-0324.1.

Kim, Y. J., S. D. Eckermann, and H. Y. Chun (2003), An overview of the past, present and future of gravity-wave drag parametrization for numerical climate and weather prediction models, *Atmos. Ocean*, *41*, 65–98, doi:10.3137/ao.410105.

Lindzen, R. S., and S. Chapman (1969), Atmospheric tides, *Space science reviews*, *10*(1).

Liu, A. Z., X. Lu, and S. J. Franke (2013), Diurnal variation of gravity wave momentum flux and its forcing on the diurnal tide, *J. Geophys. Res.: Atmospheres*, *118*(4), 1668–

1678, doi:10.1029/2012JD018653.

Liu, H. L., J. M. McInerney, S. Santos, P. H. Lauritzen, M. A. Taylor, and N. M. Pedatella (2014), Gravity waves simulated by high-resolution whole atmosphere community climate model, *Geophys. Res. Lett.*, *41*, 9106–9112, doi:10.1002/2014GL062468.

Lott, F., and C. Guez (2013), A stochastic parameterization of the gravity waves due to convection and its impact on the equatorial stratosphere, *J. Geophys. Res.: Atmospheres*, *118*, 88978909, doi:10.1002/jgrd.50705.

Marsh, D. R., D. M.J. Mills, J.-F. Kinnison, N. C. Lamarque, and L. M. Polvani (2013), Climate change from 1850 to 2005 simulated in cesm1(waccm), *J. of Climate*, *26*(19), doi:10.1175/JCLI-D-12-00558.1.

Meyer, C. K. (1999), Gravity wave interactions with the diurnal propagating tide, *J. Geophys. Res.: Atmospheres*, *104*(D4), 4223–4239, doi:10.1029/1998JD200089.

Muraschko, J., M. D. Fruman, U. Achatz, S. Hickel, and Y. Toledo (2015), On the application of wentzelkramerbrillouin theory for the simulation of the weakly nonlinear dynamics of gravity waves, *Q. J. R. Meteorol. Soc.*, doi:10.1002/qj.2381.

Plougonven, R., and F. Zhang (2014), Internal gravity waves from atmospheric jets and fronts, *Rev. Geophys.*, *52*(1), doi:10.1002/2012RG000419.

Ribstein, B., F. Senf, and U. Achatz (2015), The interaction between gravity waves and solar tides: Results from 4-d ray tracing coupled to a linear tidal model, *J. Geophys. Res.: Space Physics*, *120*(8), doi:10.1002/2015JA021349.

Riggin, D. M., T. Tsuda, and A. Shinbori (2016), Evaluation of momentum flux with radar, *Journal of Atmospheric and Solar-Terrestrial Physics*, *142*, 98–107, doi: 10.1016/j.jastp.2016.01.013.

Schmidt, H., et al. (2006), The HAMMONIA chemistry climate model: sensitivity of the mesopause region to the 11-year solar cycle and co_2 doubling, *J. Climate*, *19*(16), 3903–3931, doi:10.1175/JCLI3829.1.

Senf, F., and U. Achatz (2011), On the impact of middle-atmosphere thermal tides on the propagation and dissipation of gravity waves, *J. Geophys. Res.: Atmospheres*, *116*(D24), doi:10.1029/2011JD015794.

Sutherland, B. R. (2001), Finite-amplitude internal wavepacket dispersion and breaking, *J. Fluid Mech.*, *429*, 343–380, doi:10.1017/S0022112000002846.

Vanneste, J. (2013), Balance and spontaneous wave generation in geophysical flows, *Ann. Rev. Fluid Mech.*, *45*, 147–172, doi:10.1146/annurev-fluid-011212-140730.

Zhang, X., J. M. Forbes, M. E. Hagan, J. M. Russell, S. E. Palo, C. J. Mertens, and M. G. Mlynczak (2006), Monthly tidal temperatures 20120 km from TIMED/SABER, *J. Geophys. Res.: Space Physics*, *111*(A10), doi:10.1029/2005JA011504.

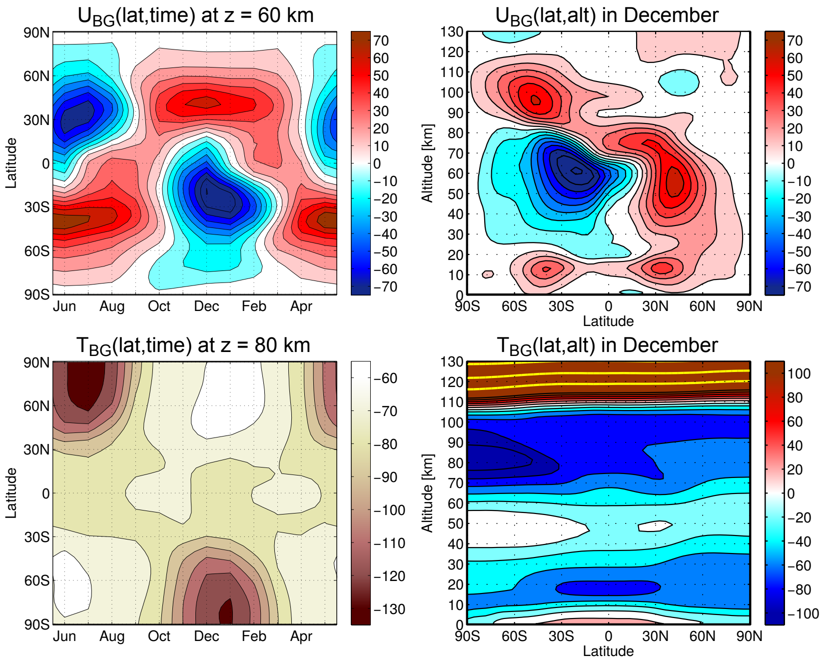

Figure 1. Annual cycle at two selected altitudes (left column) and December altitude-latitude representation (right column) of the zonal-mean HAMMONIA data, used in the present study as monthly-mean climatological fields in the background flow. Shown are the wind (top row) and the temperature (bottom row) with additional yellow isolines at $(200; 300; 400)^0C$.

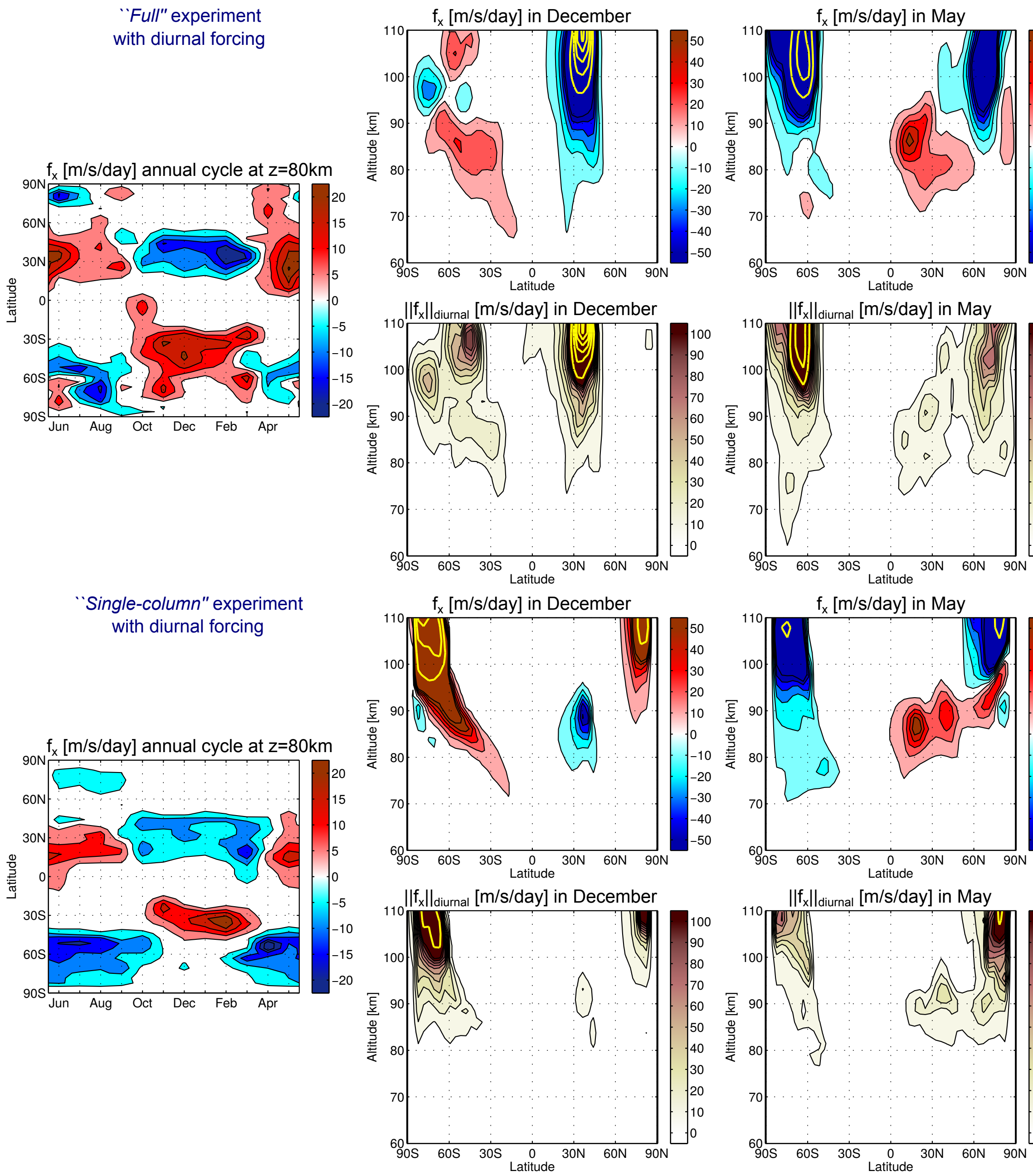

Figure 2. Zonal mean of the daily mean (1^{st} and 3^{rd} row) and the diurnal amplitude (2^{nd} and 4^{th} row) of the GW zonal acceleration f_x from simulations with purely diurnal climatological forcing in the linear tidal model. The 1^{st} and 2^{nd} row show results obtained from the ray tracer without simplification, while the 3^{rd} and 4^{th} show results in single-column approximation. Additional yellow isolines have been added at $\pm[150; 300; 450; 600]m/s/day$. The left column shows the annual cycle at $80km$, the middle and right columns latitude-altitude profiles of the results for December and May conditions, respectively.

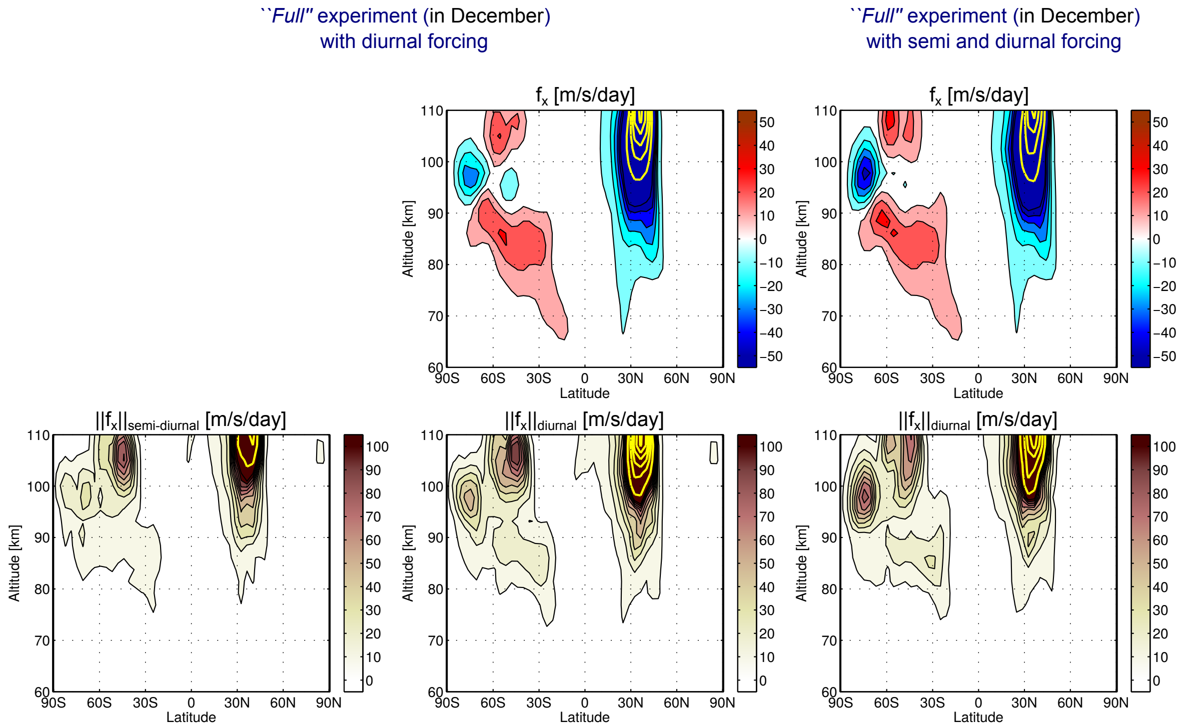

Figure 3. Zonal mean of the daily mean (top row) and of the (semi)diurnal amplitude (bottom row) of the GW zonal acceleration f_x from simulations with purely diurnal (left and middle columns) or with semi-diurnal and diurnal (right column) climatological forcing in the linear tidal model. Shown are results from the ray tracer without simplification, under December conditions. Additional yellow isolines at $\pm[150; 300; 450; 600] m/s/day$.

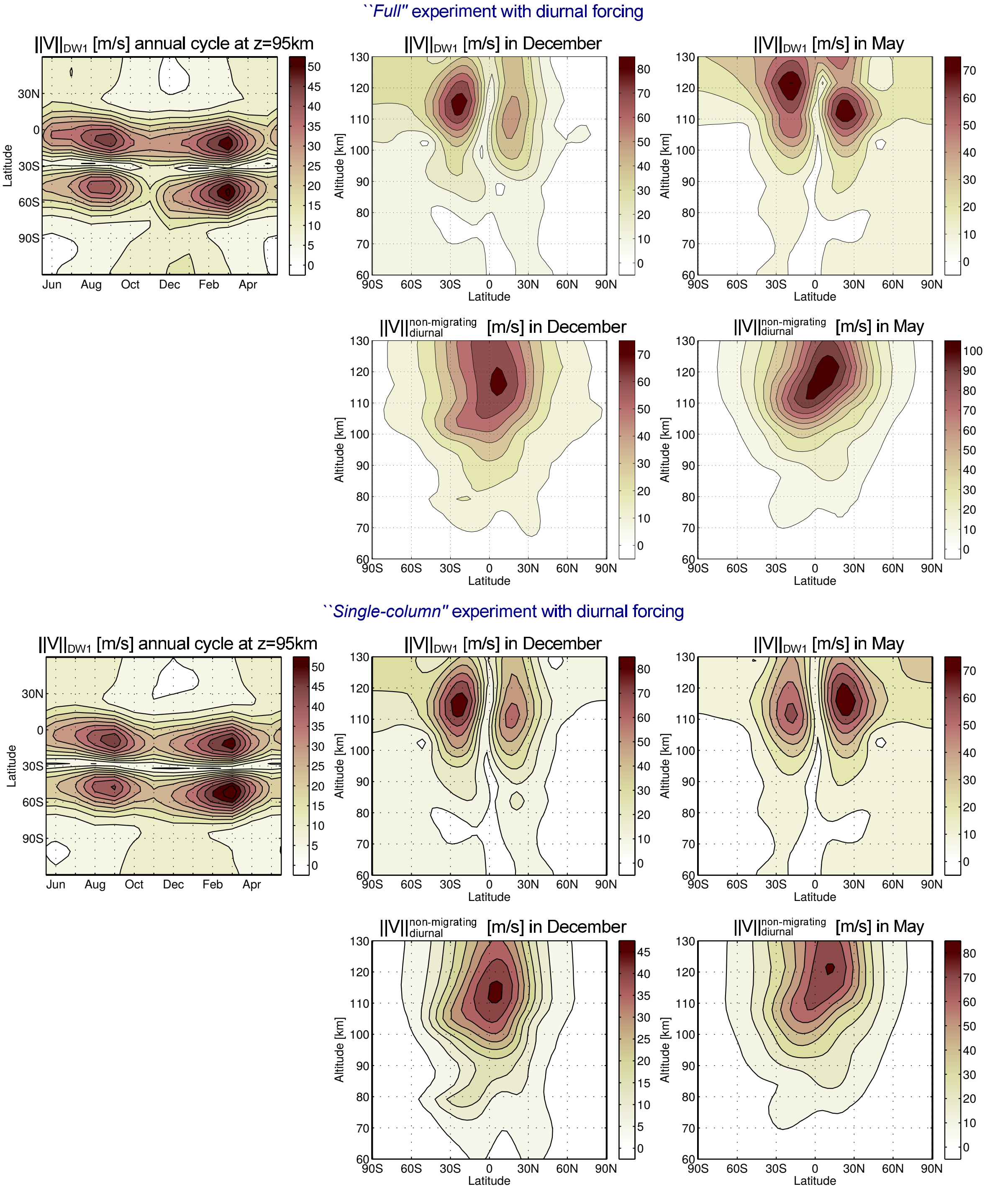

Figure 4. For the meridional-wind, the amplitude of the diurnal migrating DW_1 ST (1^{st} and 3^{rd} row) and the zonal-mean amplitude of the non-migrating STs (2^{nd} and 4^{th}), from simulations with purely diurnal climatological heating in the linear tidal model. The 1^{st} and 2^{nd} row show results obtained when the ray tracer is run without simplification, the 3^{rd} and 4^{th} results from corresponding single column experiments. The left column shows the annual cycle of the migrating ST at $95km$, and the middle and right columns latitude-altitude profiles for December and May, respectively. Note the difference in contour lines and color shading between rows 2 and 4.

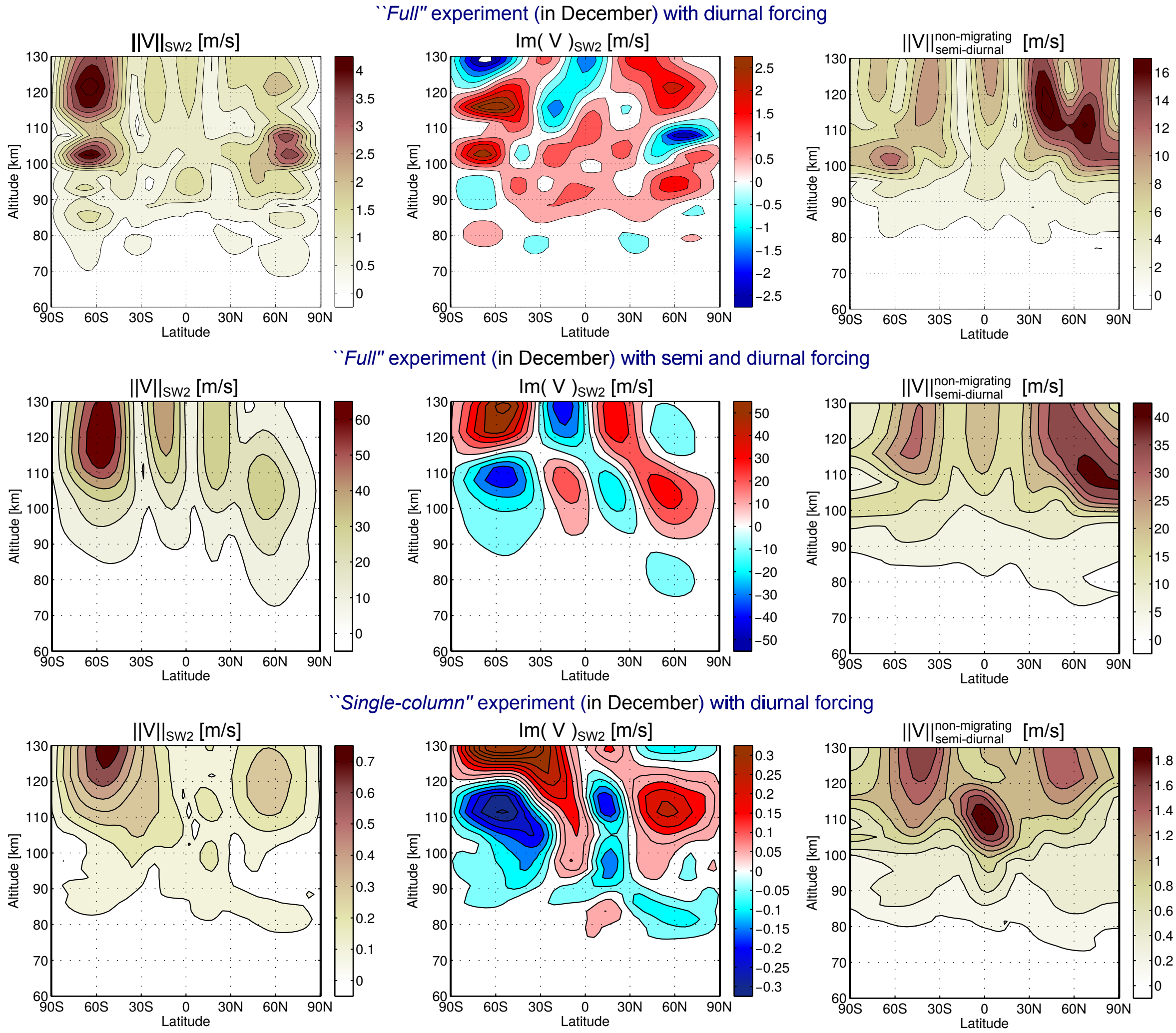

Figure 5. For the meridional wind in the December semi-diurnal ST, the amplitude of the migrating component (left and middle column) and the zonal-mean amplitude of the non-migrating part (right). The top and bottom row show results from simulations with purely diurnal heating, and the middle row those from simulations with both diurnal and semi-diurnal heating in the tidal model. The top and middle row show results from the unsimplified coupled model, and the bottom row those obtained with the single-column approximation.

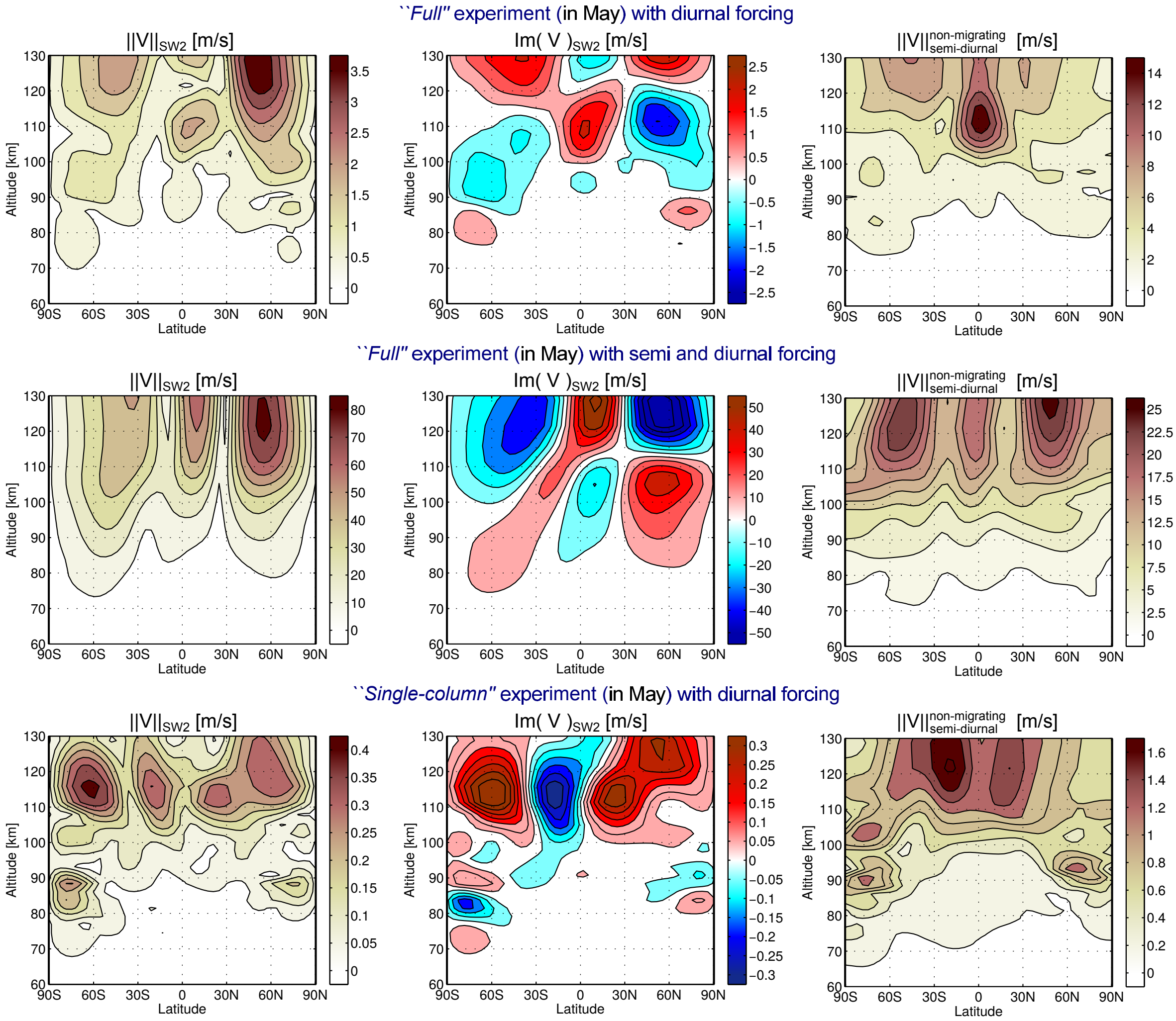

Figure 6. As in Fig. 6 but for May.

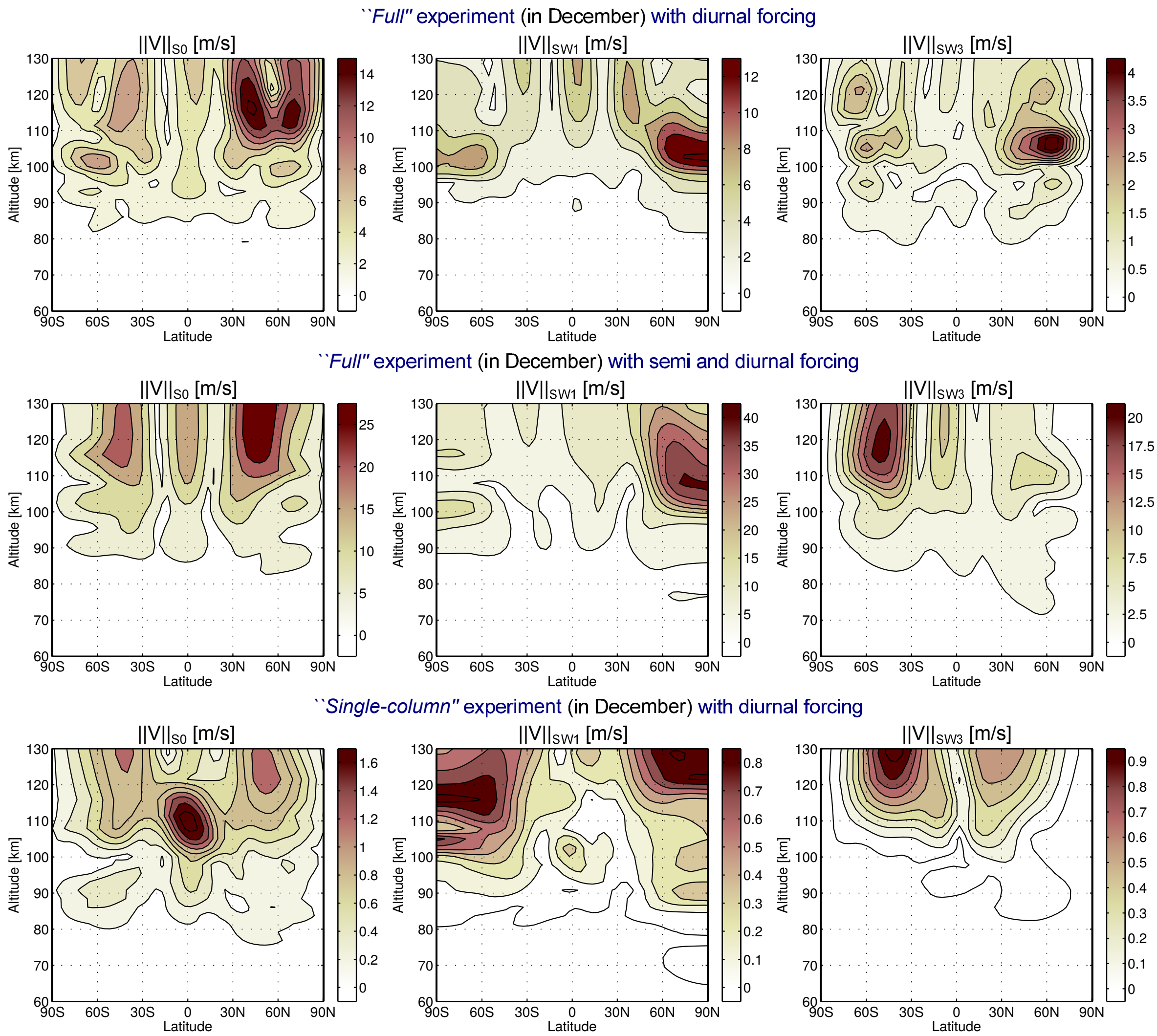

Figure 7. For the meridional wind in the December semi-diurnal ST, the amplitude of different non-migrating components : S_0 (left column), SW_1 (middle column) and SW_3 (right column). The top and bottom row show results from simulations with purely diurnal heating, and the middle row those from simulations with both diurnal and semi-diurnal heating in the tidal model. The top and middle row show results from the unsimplified coupled model, and the bottom row those obtained with the single-column approximation.